Large enhancement in thermoelectric efficiency of quantum dot junctions due to increase of level degeneracy

David M. T. Kuo,[1,*] Chih-Chieh Chen,[2] and Yia-Chung Chang[3,4,†]

[1]*Department of Electrical Engineering and Department of Physics, National Central University, Chungli, 320 Taiwan*

[2]*Department of Physics, Zhejiang University, Hangzhou 310027 China*

[3]*Research Center for Applied Sciences, Academic Sinica, Taipei, 11529 Taiwan*

[4]*Department of Physics, National Cheng Kung University, Tainan, 701 Taiwan*

(Received 8 October 2016; revised manuscript received 30 January 2017; published 27 February 2017)

It is theoretically demonstrated that the figure of merit (ZT) of quantum dot (QD) junctions can be significantly enhanced when the degree of degeneracy of the energy levels involved in electron transport is increased. The theory is based on the the Green-function approach in the Coulomb blockade regime by including all correlation functions resulting from electron-electron interactions associated with the degenerate levels (L). We found that electrical conductance (G_e) as well as electron thermal conductance (κ_e) are highly dependent on the level degeneracy (L), whereas the Seebeck coefficient (S) is not. Therefore, the large enhancement of ZT is mainly attributed to the increase of G_e when the phonon thermal conductance (κ_{ph}) dominates the heat transport of the QD junction system. In the serially coupled double-QD case, we also obtain a large enhancement of ZT arising from higher L. Unlike G_e and κ_e, S is found almost independent on electron interdot hopping strength.

DOI: 10.1103/PhysRevB.95.075432

I. INTRODUCTION

Recently, many efforts have been devoted to the search of high-efficiency thermoelectric (TE) materials because of the high demand of energy-saving solid state coolers and power generators [1,2]. TE devices have very good potential for green energy applications due to their desirable features, including low air pollution, low noise, and long operation time. However, there exists certain barriers for TE devices to replace conventional refrigerators and power generators since TE materials with figure of merit (ZT) larger than three are not yet found [1,2]. The figure of merit, $ZT = S^2 G_e T/\kappa$, defined in the linear response regime is composed of the Seebeck coefficient (S), electrical conductance (G_e), thermal conductance (κ), and equilibrium temperature (T). κ is the sum of the electron thermal conductance (κ_e) and phonon thermal conductance (κ_{ph}). It has been shown that low-dimensional systems including quantum wells [3], quantum wires [4], and quantum dots (QDs) [5] have very impressive ZT values when compared with bulk materials [3–9]. In particular, ZT of the PbSeTe QD array (QDA) can reach two [5], which is mainly attributed to the reduction of κ_{ph} in QDA [2]. However, QD junctions with $ZT \geqslant 3$ are not yet reported experimentally. There are some technical difficulties in using the QD junction to achieve $ZT \geqslant 3$ via the reduction of phonon thermal conductivity [1,2].

More than two decades ago, Hicks and Dresselhauss theoretically predicted that ZT values of BiTe quantum wells and quantum wires can be larger than one at room temperature [10,11]. In particular, ZT values of nanowires (with diameter smaller than 1 nm) may reach 10 based on the assumption of very low lattice thermal conductivity ($\kappa_L = 1.5 W m^{-1} K^{-1}$ for Bi_2Te_3). Recently, there has been considerable interest in ZT values of nanowires filled with QDs [1,2], because it is expected that κ_{ph} can be reduced significantly due to the introduction of QDs. Such a reduction of κ_{ph} due to phonon scattering with QDs in SiGe nanowire filled with QDs was verified theoretically in Ref. [12]. However, the behaviors of G_e, S, and κ_e in nanowires filled with QDs remain unclear because of the complicated many-body problem involved. The full many-body effect on the behaviors of electron thermoelectric coefficients may be analyzed by considering a single QD or double QDs (DQD) embedded in a single nanowire to reveal the importance of the electron Coulomb interaction.

Theoretical studies have indicated that a TE device made of molecular QD junction [13,14] can reach the Carnot efficiency if one can neglect κ_{ph}. Such a divergence of ZT for QDs is related to the divergence of G_e/κ_e, which violates the Wiedeman-Franz law (WFL) [15]. The violation of WFL is a typical feature for QDs with discrete energy levels [16]. It is hard to realize thermal devices with Carnot efficiency as considered in Refs. [13,14], because it is impossible to blockade acoustic phonon heat flow completely in the implementation of solid state TE devices [1,2]. Therefore, finding a way to enhance ZT of QD junctions under an achievable κ_{ph} value is crucial. Here, we demonstrate that by increasing the level degeneracy in QDs, it is possible to enhance the thermoelectric efficiency significantly given the condition $\kappa_{ph}/\kappa_e \gg 1$. The level degeneracy in a QD can be determined by its point-group symmetry. For spherical QDs made of semiconductors with zincblende (e.g., III-V compounds) or diamond crystal structure (e.g., Si or Ge), the point group is Td. Thus, the orbital degeneracy L can be described by singlet (A_1), doublet (E_2), or triplet (T_2). If the QD energy levels are well described by the effective-mass model (neglecting the crystal-field effect), then the orbital degeneracy is determined by the associated orbital angular momentum quantum number ℓ, and the level degeneracy becomes $L = 2\ell + 1$. For example, the p-like states in a spherical QD are threefold degenerate with $L = 3$ (not including spin degeneracy). In an QD junction, one can tune the gate voltage to access the level with desired

*mtkuo@ee.ncu.edu.tw

†yiachang@gate.sinica.edu.tw

degeneracy. The high level degeneracy (L) is also feasible in QDs made of multivalley semiconductors such as Si or Ge. Our theoretical results may serve as a useful guideline for optimizing ZT of semiconductor QD [1,2] or molecular QD systems [13], in which a dominating phonon thermal conductivity cannot be avoided.

II. FORMALISM

Here we consider nanoscale semiconductor QDs embedded in a nanowire connected with metallic electrodes. An extended Anderson model is employed to simulate a QD junction with degenerate levels [17–19]. The Hamiltonian of the QD junction system considered is given by $H = H_0 + H_{QD}$, where

$$H_0 = \sum_{k,\sigma} \epsilon_k a^\dagger_{k,\sigma} a_{k,\sigma} + \sum_{k,\sigma} \epsilon_k b^\dagger_{k,\sigma} b_{k,\sigma} + \sum_{k,\ell,\sigma} V^L_{k,\ell} d^\dagger_{\ell,\sigma} a_{k,\sigma} + \sum_{k,\ell,\sigma} V^R_{k,\ell} d^\dagger_{\ell,\sigma} b_{k,\sigma} + \text{c.c.} \quad (1)$$

The first two terms of Eq. (1) describe the free electron gas in the left and right electrodes. $a^\dagger_{k,\sigma}$ ($b^\dagger_{k,\sigma}$) creates an electron of momentum k and spin σ with energy ϵ_k in the left (right) electrode. $V^L_{k,\ell}$ ($V^R_{k,\ell}$) describes the coupling between the ℓth energy level of the QD system and left (right) electrode. $d^\dagger_{\ell,\sigma}$ ($d_{\ell,\sigma}$) creates (destroys) an electron in the ℓth energy level of the QD.

$$H_{QD} = \sum_{\ell,\sigma} E_\ell n_{\ell,\sigma} + \sum_{\ell} U_\ell n_{\ell,\sigma} n_{\ell,\bar{\sigma}} + \frac{1}{2} \sum_{\ell,j,\sigma,\sigma'} U_{\ell,j} n_{\ell,\sigma} n_{j,\sigma'}, \quad (2)$$

where E_ℓ is the spin-independent QD energy level, and $n_{\ell,\sigma} = d^\dagger_{\ell,\sigma} d_{\ell,\sigma}$, U_ℓ, and $U_{\ell,j}$ describe the intralevel and interlevel Coulomb interactions, respectively. For nanoscale semiconductor QDs, the interlevel Coulomb interactions as well as intralevel Coulomb interactions play a significant role on the electron transport in semiconductor junctions. It is worth noting that H_{QD} possesses the particle-hole symmetry. One can prove it with a simple swap of electron and hole operators ($d_{\ell,\sigma} \to c^\dagger_{\ell,\sigma}$). The form of H_{QD} is changed only by constant terms when QD energy levels are degenerate. This indicates that dynamic physical quantity is unchanged in the hole picture.

To reveal the transport properties of a QD junction connected with metallic electrodes, it is convenient to use the Green-function technique. The electron and heat currents from reservoir α to the QD are calculated according to the Meir-Wingreen formula [19]

$$J^n_\alpha = \frac{ie}{h} \sum_{j\sigma} \int d\epsilon \left(\frac{\epsilon - \mu_\alpha}{e}\right)^n \Gamma^\alpha_j \times \left[G^<_{j\sigma}(\epsilon) + f_\alpha(\epsilon)\left(G^r_{j\sigma}(\epsilon) - G^a_{j\sigma}(\epsilon)\right)\right], \quad (3)$$

where $n = 0$ is for the electrical current and $n = 1$ for the heat current. $\Gamma^\alpha_j(\epsilon) = \sum_k |V_{k,j}|^2 \delta(\epsilon - \epsilon_k)$ is the tunneling rate for electrons from the αth reservoir and entering the jth energy level of the QD. $f_\alpha(\epsilon) = 1/\{\exp[(\epsilon - \mu_\alpha)/k_B T_\alpha] + 1\}$ denotes the Fermi distribution function for the αth electrode, where μ_α and T_α are the chemical potential and the temperature of the α electrode. e, h, and k_B denote the electron charge, the Planck's constant, and the Boltzmann constant, respectively. $G^<_{j\sigma}(\epsilon)$, $G^r_{j\sigma}(\epsilon)$, and $G^a_{j\sigma}(\epsilon)$ denote the frequency-domain representations of the one-particle lessor, retarded, and advanced Green's functions, respectively.

A. Thermoelectric coefficients

Thermoelectric coefficients including G_e, S, and κ_e in the linear response regime can be evaluated by using Eq. (3) with small $\Delta V = (\mu_L - \mu_R)/e$ and $\Delta T = T_L - T_R$. We obtain the following expressions of thermoelectric coefficients:

$$G_e = \left(\frac{\delta J^0_\alpha}{\delta \Delta V}\right)_{\Delta T=0} \quad (4)$$

$$S = -\left(\frac{\delta J^0_\alpha}{\delta \Delta T}\right)_{\Delta V=0} \Big/ \left(\frac{\delta J^0_\alpha}{\delta \Delta V}\right)_{\Delta T=0} \quad (5)$$

$$\kappa_e = \left(\frac{\delta J^1_\alpha}{\delta \Delta T}\right)_{\Delta V=0} + \left(\frac{\delta J^1_\alpha}{\delta \Delta V}\right)_{\Delta T=0} S = \left(\frac{\delta J^1_\alpha}{\delta \Delta T}\right)_{\Delta V=0} - S^2 G_e T, \quad (6)$$

where

$$\left(\frac{\delta J^0_\alpha}{\delta \Delta V}\right)_{\Delta T=0} = \frac{ie}{h} \sum_{j\sigma} \int d\epsilon \Gamma^\alpha_j(\epsilon) \times \left[\frac{\delta G^<_{j\sigma}(\epsilon)}{\delta f_\alpha(\epsilon)} + \left(G^r_{j\sigma}(\epsilon) - G^{(a}_{j\sigma}(\epsilon)\right)\right] \frac{\delta f_\alpha(\epsilon)}{\delta \Delta V}, \quad (7)$$

$$\left(\frac{\delta J^0_\alpha}{\delta \Delta T}\right)_{\Delta V=0} = \frac{ie}{h} \sum_{j\sigma} \int d\epsilon \Gamma^\alpha_j(\epsilon) \times \left[\frac{\delta G^<_{j\sigma}(\epsilon)}{\delta f_\alpha(\epsilon)} + \left(G^r_{j\sigma}(\epsilon) - G^{(a}_{j\sigma}(\epsilon)\right)\right] \frac{\delta f_\alpha(\epsilon)}{\delta \Delta T}, \quad (8)$$

$$\left(\frac{\delta J^1_\alpha}{\delta \Delta T}\right)_{\Delta V=0} = \frac{i}{h} \sum_{j\sigma} \int d\epsilon \Gamma^\alpha_j(\epsilon)(\epsilon - E_F) \times \left[\frac{\delta G^<_{j\sigma}(\epsilon)}{\delta f_\alpha(\epsilon)} + \left(G^r_{j\sigma}(\epsilon) - G^a_{j\sigma}(\epsilon)\right)\right] \frac{\delta f_\alpha(\epsilon)}{\delta \Delta T}, \quad (9)$$

$$\left(\frac{\delta J^1_\alpha}{\delta \Delta V}\right)_{\Delta T=0} = \frac{i}{h} \sum_{j\sigma} \int d\epsilon \Gamma^\alpha_j(\epsilon)(\epsilon - E_F) \times \left[\frac{\delta G^<_{j\sigma}(\epsilon)}{\delta f_\alpha(\epsilon)} + \left(G^r_{j\sigma}(\epsilon) - G^a_{j\sigma}(\epsilon)\right)\right] \frac{\delta f_\alpha(\epsilon)}{\delta \Delta V}. \quad (10)$$

$\frac{\delta G^<_{j\sigma}(\epsilon)}{\delta f_\alpha(\epsilon)}$ is obtained by taking the derivative of the equation of motion with respect to the change in Fermi-Dirac distribution, $f_\alpha(\epsilon)$. Here we have assumed the variation of the correlation

functions with respect to $\delta f_\alpha(\epsilon)$ is of the second order. Note that we have to take the limit $\Delta V \to 0$ for the calculation of $(\frac{\delta J_\alpha^0}{\delta \Delta V})_{\Delta T=0}$ and $(\frac{\delta J_\alpha^1}{\delta \Delta V})_{\Delta T=0}$. E_F is the Fermi energy of electrodes. The one-particle Green's functions in Eqs. (7)–(10) are related recursively to high-order Green's functions and correlation functions via a hierarchy of equations of motion (EOM) [20]. This hierarchy self terminates at the $2N$-particle Green function, where N is the number of levels considered in the QD or coupled QDs.

To reveal the effect of degenerate levels on the thermoelectric efficiency of the QD junction system, all needed Green's functions and correlation functions arising from electron-electron interactions in the QDs considered are computed self-consistently following the procedures described in our previous work [20,21]. Our procedure is beyond the mean-field theory, which is widely used in solving the equation of motion in the Green function calculation [14]. For $L = 4$, our calculation involves solving one-, two-, $\cdots$, up to eight-particle Green functions.

B. Phonon thermal conductance

The thermoelectric efficiency of a QD junction embedded in a nanowire is determined by the figure of merit, $ZT = S^2 G_e T/(\kappa_e + \kappa_{ph})$, which involves the κ_{ph} of the QD junction system. The optimization of molecular QD junctions under the condition of $\kappa_e/\kappa_{ph} \gg 1$ has been theoretically investigated in Refs. [13,14]. However, the condition of $\kappa_e/\kappa_{ph} \gg 1$ is very difficult to realize in practice. The main goal of this study is to investigate the effect of energy level degeneracy on thermoelectric efficiency under the realistic condition with $\kappa_{ph}/\kappa_e > 1$. The phonon thermal conductance of nanowires has been extensively studied experimentally and theoretically [22–32]. In Refs. [22–24] it has been shown experimentally that κ_{ph} displays a linear T behavior from 20 K to 300 K for silicon nanowires with diameter 22 nm. The linear T behavior of κ_{ph} also holds for T between 100 K and 400 K for germanium nanowires with diameter 19 nm [25]. Due to the reduction of κ_{ph}, ZT of silicon nanowires increases significantly (with $ZT = 1$ at 200 K) in comparison with $ZT = 0.01$ for bulk silicon at room temperature [4,26]. The linear T behavior of nanowires is an interesting topic. Many theoretical efforts have been devoted to clarifying why nanowires with diameters near 20 nm exhibit the linear T behavior [27–32]. For a true one-dimensional system, the linear T behavior of κ_{ph} is expected [33]. To include κ_{ph}, we have adopted the Landauer formula given in Refs. [28,30].

$$\kappa_{ph} = \frac{1}{h}\int d\omega \mathcal{T}(\omega)_{ph} \frac{\hbar^3\omega^2}{k_B T^2} \frac{e^{\hbar\omega/k_B T}}{(e^{\hbar\omega/k_B T}-1)^2}, \qquad (11)$$

where ω and $\mathcal{T}_{ph}(\omega)$ are the phonon frequency and throughput function, respectively. In a perfect wire throughput is unity for each open channel, then κ_{ph} in such a perfect case is given by $\kappa_{ph,0} = \frac{k_B^2\pi^2 T N_{ph}}{3h} = g_0(T)N_{ph}$, where N_{ph} is the total number of open modes and $g_0(T) = \frac{k_B^2\pi^2}{3h}T = 9.456 \times 10^{-4} T(nW/K^2)$ is called the quantum conductance [34]. Experimentally, it was found that the linear-T behavior in the ballistic regime only holds for temperature below 0.8 K for wires of size 200 nm with $N_{ph} = 4$ (which includes one longitudinal, one torsional, and two flexural modes) [34]. Beyond 0.8 K, the nonlinear-T behavior was observed due the contribution of high-energy phonon modes being thermally populated. Low-temperature thermoelectric properties of Kondo insulator nanowire were also studied in Ref. [35] by using the Callaway model to describe κ_{ph}.

If there exists phonon elastic scattering from the disorder effects of nanowire surface [27–33] or interface boundary of QDs embedded in the nanowire [36,37], the throughput function becomes more complicated [27–33]. In general, the $\mathcal{T}_{ph}(\omega)$ depends on the length ($\tilde{L}$) and diameter (D) of the nanowire, phonon mean free path $\ell_0(\omega)$, and Debye frequency (ω_D). Realistic calculation of $\mathcal{T}_{ph}$ requires heavy numerical work for treating the detailed phonon dispersion curves [29–33,36,37], which is beyond the scope of this paper. However, an empirical expression which works well in general for semiconductor nanowires at a wide range of temperature can be found in Ref. [24], which reads

$$\mathcal{T}_{ph}(\omega) = \frac{N_{ph,1}(\omega)}{1+\tilde{L}/\ell_0(\omega)} + \frac{N_{ph,2}(\omega)}{1+\tilde{L}/D} \qquad (12)$$

with the frequency-dependent mean free path $\ell_0(\omega)$ given by

$$\frac{1}{\ell_0(\omega)} = B\frac{\delta^2}{D^3}\left(\frac{\omega}{\omega_D}\right)^2 N_{ph}(\omega), \qquad (13)$$

where $N_{ph}(\omega) = 4 + A(\frac{D}{a})^2(\frac{\omega}{\omega_D})^2$ (for $\omega < \omega_D$) denotes the number of phonon modes, and a denotes the lattice constant of the nanowire material. A and B are dimensionless parameters chosen to be [24] $A = 2.17$ and $B = 1.2$. $N_{ph,1}(\omega) = N_{ph}(min(\omega, v_s/\delta))$ and $N_{ph,2}(\omega) = N_{ph}(\omega) - N_{ph,1}(\omega)$. v_s is the sound velocity of the nanowire and δ describes the thickness of the rough surface of the nanowire [24,28]. In Eq. (12), one essentially replaces the frequency-dependent mean free path $\ell_0(\omega)$ by a constant D for the high-frequency modes ($\omega > v_s/\delta$).

For a certain range of temperatures, a simple expression of $\kappa_{ph}(T)$ for the molecular QD junction system may be used. One can approximately write [13]

$$\kappa_{ph} = F_s g_0(T), \qquad (14)$$

where F_s is a dimensionless correction factor used to describe the effect of nonballistic phonon transport due to surface roughness and phonon scattering from QDs, which replaces the throughput function $\mathcal{T}_{ph}(\omega)$ used in Eq. (11). The simple expression of Eq. (14) with $F_s = 0.1$ will be used to describe κ_{ph} throughout this paper except in Fig. 4. In Fig. 4, we compare ZT as a function of temperature obtained by using both Eq. (12) and Eq. (14). It is found that with the simple scaling factor F_s we can describe the behavior of κ_{ph} reasonably well for thin nanowires in the temperature range of interest. With this simple scaling we can clarify the effect of level degeneracy (L) on ZT for different magnitudes of κ_{ph}.

III. RESULTS AND DISCUSSION

Based on Eqs. (4)–(6), we numerically calculate thermoelectric coefficients including all correlation functions arising from electron Coulomb interactions in the QDs. Figure 1 shows ZT of a single QD junction as a function of the QD level E_0, which is tuned by gate voltage V_g according

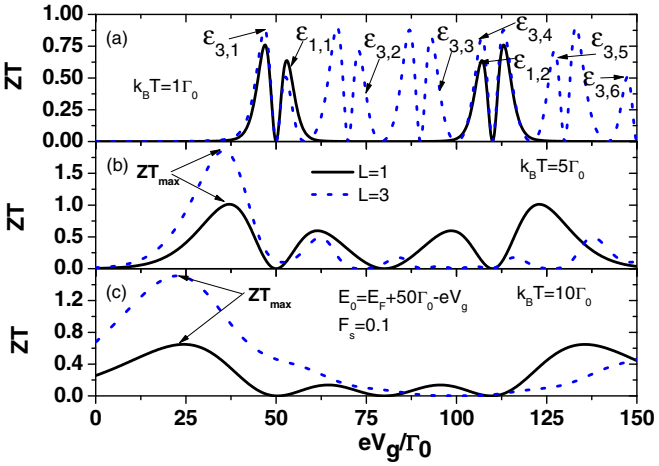

FIG. 1. Figure of merit as a function of QD energy level tuned by gate voltage ($E_0 = E_F + 50\Gamma_0 - eV_g$) for level degeneracy, $L = 1$ and 3. (a) $k_BT = 1\Gamma_0$, (b) $k_BT = 5\Gamma_0$, and (c) $k_BT = 10\Gamma_0$. The correction factor for phonon scattering is $F_s = 0.1$. We have adopted the intralevel Coulomb interaction $U_0 = 60\Gamma_0$ for $L = 1$ and $U_0 = U_I = 20\Gamma_0$ for $L = 3$. U_I denotes the interlevel Coulomb interaction.

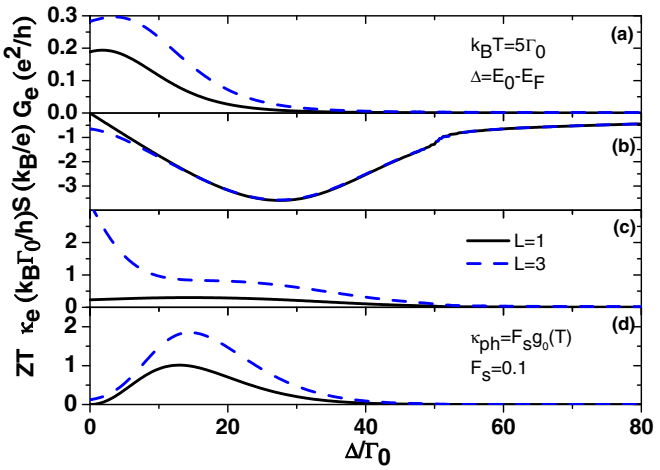

FIG. 2. (a) Electrical conductance (G_e), (b) Seebeck coefficient (S), (c) electron thermal conductance (κ_e), and (d) figure of merit (ZT) as a function of QD energy energy level ($\Delta = E_0 - E_F$) for different orbital degenerated states at $k_BT = 5\Gamma_0$. $F_s = 0.1$ was used in the calculation of ZT.

to $E_0 = E_F + 50\Gamma_0 - eV_g$ for the case of nondegeneracy ($L = 1$) and threefold degeneracy ($L = 3$). Note that the role of gate voltage introduced here allows us to tune the difference between the QD level energy and Fermi energy. Throughout this paper, we adopt a symmetrical tunneling rate with $\Gamma_L = \Gamma_R = \Gamma = \Gamma_0$ and all energy scales are in terms of Γ_0. $\Gamma_0 \approx 1$ meV in typically QD junctions; thus, reasonable values for U_0 and U_I in realistic semiconductor QDs are in the range of 20–100 Γ_0. Figures 1(a)–1(c) are for $k_BT = 1\Gamma_0$, $k_BT = 5\Gamma_0$, and $k_BT = 10\Gamma_0$, respectively. It is seen that the maximum ZT for the threefold case is significantly higher than the corresponding value for the nondegenerate case when the temperature is high. For example, the maximum ZT [labeled by $(ZT)_{\max}$ is enhanced by nearly two times for $k_BT = 5\Gamma_0$ and more than two times for $k_BT = 10\Gamma_0$, although the enhancement of ZT for $L = 3$ is small at $k_BT = 1\Gamma_0$. We observe several new spectral features with similar ZT values at E_0 values spaced apart approximately by the charging energy U_0 or U_I, which is caused by the intralevel and interlevel Coulomb interactions. For the nondegenerate case ($L = 1$), thermoelectric coefficients can be calculated in terms of the transmission coefficient $\mathcal{T}_{LR}(\epsilon)$, which can be expressed as

$$\frac{\mathcal{T}_{LR}(\epsilon)}{4\Gamma_L\Gamma_R} = \frac{1 - N_{-\sigma}}{(\epsilon - E_0)^2 + \bar{\Gamma}^2} + \frac{N_{-\sigma}}{(\epsilon - E_0 - U_0)^2 + \bar{\Gamma}^2}, \quad (15)$$

where $\bar{\Gamma} = \Gamma_L + \Gamma_R$, and $N_{-\sigma}$ denotes the single-particle occupation number. Equation (15) illustrates two resonant peaks at $\epsilon = E_0$ and $\epsilon = E_0 + U_0$ with the probability weights of $(1 - N_{-\sigma})$ and $N_{-\sigma}$, respectively, which are related to the two M-shaped spectral features in ZT (labeled by $\epsilon_{1,1}$ and $\epsilon_{1,2}$) with the dip position corresponding to the resonance energies. (Here the intralevel Coulomb interaction used is $U_0 = 60\Gamma_0$.) Similarly, for $L = 3$ at $k_BT = 1\Gamma_0$ we label the six M-shaped spectral features by $\epsilon_{3,n}$ ($n = 1, \cdots 6$), which result from the resonant channels at E_0, $E_0 + U_I$, $E_0 + 2U_I$, $E_0 + U_0 + 2U_I$, $E_0 + U_0 + 3U_I$, and $E_0 + U_0 + 4U_I$, respectively. (Here, we have adopted $U_0 = U_I = 20\Gamma_0$. U_I denotes the interlevel Coulomb interactions for the $L = 3$ case.) These channels correspond to physical processes of filling the QD with one to six electrons. At higher temperatures ($k_BT = 5\Gamma_0$ and $k_BT = 10\Gamma_0$), the first M-shaped spectral feature for ZT is broadened and enlarged. (The last M-shaped ZT feature for $L = 3$ is not shown in Fig. 1. For $L = 3$, the other spectral features of ZT (at $\epsilon_{3,n}$; $n = 2,3,4,5$) are suppressed. This is attributed to the significant reduction of maximum S^2 for those channels. Because of electron-hole symmetry in the system Hamiltonian, it is expected that the spectrum of ZT is symmetrical about the middle point of the Coulomb gap (MPCG). For $L = 3$, MPCG occurs at $eV_g = 100\Gamma_0$. Therefore, we only need to focus on the analysis of ZT optimization near the first spectral feature in the level-depletion regime, which is defined as the regime when the average occupation number of the QD summed over spin (N_t) is less than one. In general, it occurs at $E_0 > E_F$.

To gain a better understanding of the enhancement mechanism for $(ZT)_{\max}$ resulting from increased degeneracy, we calculate the G_e, S, κ_e, and ZT of the QD junction as functions of the level energy ($\Delta = E_0 - E_F$) at $k_BT = 5\Gamma_0$ for $L = 1$ and $L = 3$, and the results are shown in Fig. 2. In Fig. 2(a) the maximum G_e value is enhanced with increasing of degeneracy, although its dependence of L is not linear. This is mainly attributed to complicated correlation functions arising from the electron Coulomb interactions in QD. G_e is much smaller than $G_0 = \frac{2e^2}{h}$ (the electron quantum conductance) even for $L = 3$, which is mainly attributed to strong electron Coulomb interactions. We note that the Seebeck coefficient is almost independent of L, whereas G_e and κ_e are enhanced with increasing L. However, since $\kappa_{ph}/\kappa_e \gg 1$, the L dependence of κ_e won't affect ZT appreciably. Thus, the enhancement of ZT shown in Fig. 1(b) mainly comes from the increase of G_e, not S. In the Coulomb blockade regime, κ_e and G_e are highly suppressed. Thus, if one can introduce a mechanism to reduce κ_{ph} (with $F_s = 0.1$ for example), then the maximum value of

ZT can reach 1 for $L = 1$ and around 2 for $L = 3$ as illustrated in Fig. 2(d).

The calculation of thermoelectric coefficients for the $L = 3$ case including all correlation functions arising from electron Coulomb interactions is quite complicated. To reveal L-dependent $(ZT)_{\max}$, we consider the transmission coefficient $\mathcal{T}_{LR}(\epsilon)$ including only the contribution from the resonant channel $\epsilon - E_0$, which is approximately given by

$$\mathcal{T}_{LR}(\epsilon) \approx \frac{4\Gamma_L\Gamma_R L P_{L,1}}{(\epsilon - E_0)^2 + \bar{\Gamma}^2}, \tag{16}$$

where $P_{L,1}$ is the L-dependent probability weight for the resonant channel at $\epsilon = E_0$. We have $P_{3,1} = (1 - N_{-\sigma})(1 - (N_{-\sigma}+N_\sigma)+c)(1-(N_{-\sigma}+N_\sigma)+c)$, where $c = \langle n_{\ell,\sigma} n_{\ell,-\sigma}\rangle$ denotes the intralevel two particle correlation function [38].

Thermoelectric coefficients determined by the $\mathcal{T}_{LR}(\epsilon)$ of Eqs. (15) and (16) can be calculated by $G_e = e^2\mathcal{L}_0$, $S = -\mathcal{L}_1/(eT\mathcal{L}_0)$ and $\kappa_e = \frac{1}{T}(\mathcal{L}_2 - \mathcal{L}_1^2/\mathcal{L}_0)$. $\mathcal{L}_n$ is given by

$$\mathcal{L}_n = \frac{2}{h}\int d\epsilon \mathcal{T}_{LR}(\epsilon)(\epsilon - E_F)^n \frac{\partial f(\epsilon)}{\partial E_F}, \tag{17}$$

where $f(\epsilon) = 1/(exp^{(\epsilon - E_F)/k_BT} + 1)$ is the Fermi distribution function of electrodes.

Because Eq. (16) does not take into account the interlevel correlation functions arising from U_I, Eq. (16) is not adequate for illustrating thermoelectric coefficients for the situation $\Delta/k_BT \leqslant 1$. Nevertheless, we see that $(ZT)_{\max}$ of Fig. 2 does not occur in the $\Delta/k_BT \leqslant 1$ regime. Therefore, we consider the limit of weak coupling between QD and electrodes ($\Gamma_L = \Gamma_R = \Gamma \to 0$) in Eqs. (15) and (16) and obtain $G_e = \frac{G_0\Gamma\pi L P_{L,1}}{k_BT\cosh^2(\frac{\Delta}{2k_BT})}$, $S = -\Delta/(eT)$, and $\kappa_e = 0$. The L-dependent behavior of $(ZT)_{\max}$ is then determined by the simple expression

$$ZT = \frac{(\Delta/eT)^2 G_0\Gamma\pi L P_{L,1} T}{k_BT\cosh^2\left(\frac{\Delta}{2k_BT}\right)k_{ph}}, \tag{18}$$

which explains that the L-dependent ZT is determined by G_e rather than S and why ZT approaches 0 as $E_0 \to E_F$ for $L = 1$. Note that ZT for $L = 3$ does not approach zero as $\Delta \to 0$, because S has a finite value at $\Delta = 0$ [see the dashed line of Fig. 2(b)]. Such a result also indicates that the correlation arising from U_I cannot be neglected for QD when E_0 is close to E_F. Some novel nanoscale TE devices resulting from the inclusion of U_I were theoretically discussed for designing electron heat rectifiers [38] and current diodes [39].

Figure 3 shows G_e, S, κ_e, and ZT as functions of temperature with $\Delta = 15\Gamma_0$ for $L = 1,3$, and 4. From the application point of view, the temperature dependence of ZT is an important consideration for developing room temperature power generators used in consumer electronics [2]. G_e is highly enhanced for $L = 3$ and 4 in the whole temperature regime, but the difference of $L = 3$ and $L = 4$ is small, indicating a saturation behavior as L exceeds 3, mainly because of the factor $P_{L,1}$ in Eq. (16). As seen in Fig. 3(b), S is nearly independent of L for $k_BT < 7\Gamma_0$, but becomes weakly dependent on L at higher temperature. This implies that the effect of resonances at $\epsilon_{L,2}$ and $\epsilon_{L,3}$ cannot be ignored for $L > 1$ in the high temperature regime ($k_BT \geqslant 7\Gamma_0$). Although κ_e is

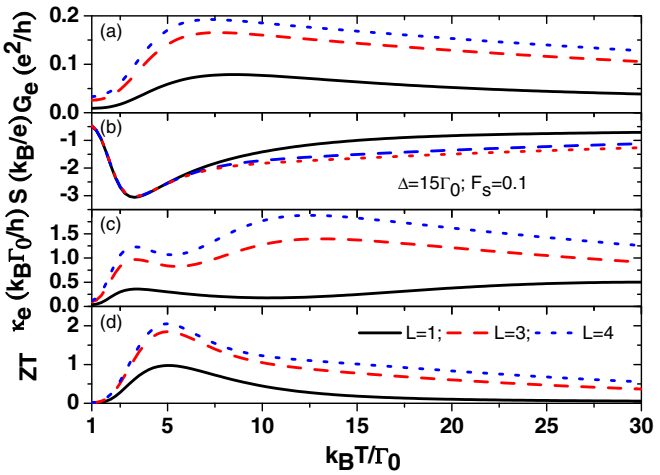

FIG. 3. (a) Electrical conductance (G_e), (b) Seebeck coefficient (S), (c) electron thermal conductance (κ_e), and (d) figure of merit (ZT) as a function of k_BT for various values of level degeneracy (L) with $\Delta = 15\Gamma_0$. Other physical parameters are the same as those of Fig. 2.

enhanced with increasing L as shown in Fig. 3(c), its effect is insignificant since κ_e is much smaller than κ_{ph}. Therefore, the behavior of ZT with respect to k_BT is determined by the power factor ($PF = S^2G_eT$). We found impressive enhancement of ZT for $L = 3$ and 4 for $k_BT \geqslant 4\Gamma_0$. Comparing Figs. 2(d) and 3(d), we see that the maximum values of ZT occur near $k_BT = \Delta/2.4$ for the tunneling rate considered ($\Gamma = 1\Gamma_0$). Based on such a condition, we can infer that the maximum ZT at room temperature $k_BT = 25$ meV will occur near $\Delta = 60$ meV for $\Gamma_0 = 1$ meV.

In Figs. 1–3, κ_{ph} is assumed to obey the simple expression give in Eq. (14). Here we examine whether the large enhancement of ZT due to level degeneracy will be destroyed when a more realistic throughput function given by Eq. (12) is considered. Figure 4 shows the comparison of ZT and κ_{ph} calculated by both Eq. (12) and Eq. (14). In Fig. 4(a),

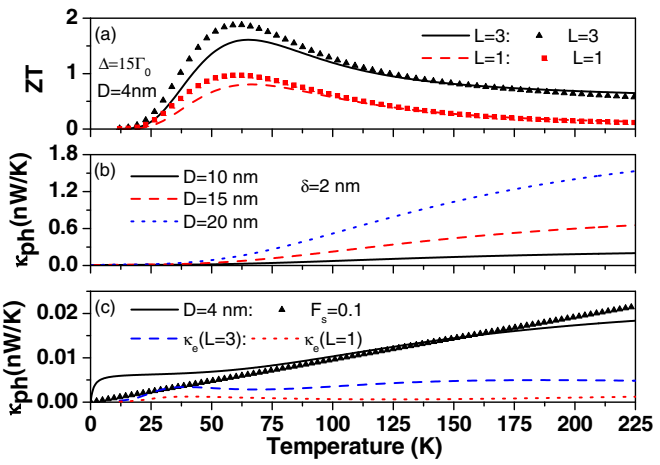

FIG. 4. (a) Figure of merit (ZT) and (b),(c) phonon thermal conductance (κ_{ph}) as a function of k_BT. The length of the nanowire used is $\tilde{L} = 2000$ nm. Other physical parameters are the same as those of Fig. 3.

κ_{ph} is used to obtain the solid ($L = 3$) and dashed curves ($L = 1$) for ZT are calculated by using Eqs. (11) and (12) with $D = 4$ nm, $\delta = 2$ nm and $\tilde{L} = 2\ \mu$m. Other parameters are given by physical properties of silicon semiconductors [24,28]. The triangle ($L = 3$) and square marks ($L = 1$) for ZT are calculated by using κ_{ph} based on Eq. (14). The maximum ZT values of solid and dashed lines are near 1.8 and 0.9, respectively. The results of Fig. 4(a) indicate that the large enhancement of ZT resulting from L is unchanged even when a more realistic expression for κ_{ph} (which is nonlinear in temperature) is used. When we compare the spectra of ZT given by the solid curve and the curve with triangle marks for the case of $L = 3$, the curves with triangle marks have better ZT value at low temperature due to the lower value of κ_{ph} in the linear-T expression. Figure 4(b) shows κ_{ph} for nanowires with diameter of 10,15, and 20 nm, which agree well with the experimental results of Ref. [24], lending support for the validity of this model. The comparison of behaviors of κ_{ph} for a 4 nm nanowire obtained by both Eq. (12) (solid curve) and Eq. (14) (triangles) is shown in Fig. 4(c). It is found that the results obtained by the simple linear-T expression of Eq. (14) are fairly close to that obtained by the realistic expression of Eq. (12) for temperatures between 50 and 200 K. In Fig. 4(c), κ_{ph} shows a nonlinear-T behavior between 1 K and 50, which is mainly attributed to frequency-dependent mean free path. The dashed and dotted lines show the behavior of electronic thermal conductance (κ_e) with respect to temperature. Note that the G_e, S, and κ_e in Fig. 4 are calculated according to the simplified method described in Ref. [38], where we only considered single-particle occupation numbers and intralevel two-particle correlation functions. The curves with triangle and square marks shown in Fig. 4(a) are almost identical to the black solid line and red dashed line of Fig. 3(d) obtained by the full calculation.

Next we examine whether the large enhancement of ZT due to increase of level degeneracy still exists in the case of coupled double QDs (DQDs). The Hamiltonian of a DQD is given by $H_{DQD} = H_{QD,L} + H_{QD,R} + U_{LR}\sum_{\ell,j} n_{L,\ell,\sigma} n_{R,j,\sigma'} + t_{LR}\sum_{\ell,j}(d^{\dagger}_{L,\ell,\sigma} d_{R,j,\sigma} + \text{H.c.})$ [40–42]. $H_{QD,L}$ ($H_{QD,R}$) denotes the Hamiltonian of the left (right) QD as defined in Eq. (2). For simplicity, the interdot electron hopping strengths (t_{LR}) and electron Coulomb interactions (U_{LR}) are assumed uniform. Although electron tunneling currents through DQDs have been extensively studied by several authors [40–42], the optimization of ZT including the effect of all correlation functions arising from electron Coulomb interactions has not been reported. Here, we assume one nondegenerate energy level for each QD ($L = 1$). The energy levels of left QD and right QD are the same (denoted E_0). Based on Eqs. (4)–(6), G_e, S, κ_e, and ZT as functions of the QD energy level (which is related to the gate voltage by $E_0 = E_F + 50\Gamma_0 - eV_g$) for $K_BT = 3$, 5, and 7 Γ_0 are plotted in Fig. 5. There are four peaks labeled by $\epsilon_{1,n}$ ($n = 1,2,3,4$) in the spectrum of electrical conductance (G_e). The Seebeck coefficient (S) behaves like the derivative of $-G_e$ and is vanishingly small at the MPCG due to electron-hole symmetry. The maximum S occurs near the onset of the first peak in G_e or the ending of the last peak. Both κ_e and G_e are symmetrical with respect to MPCG.

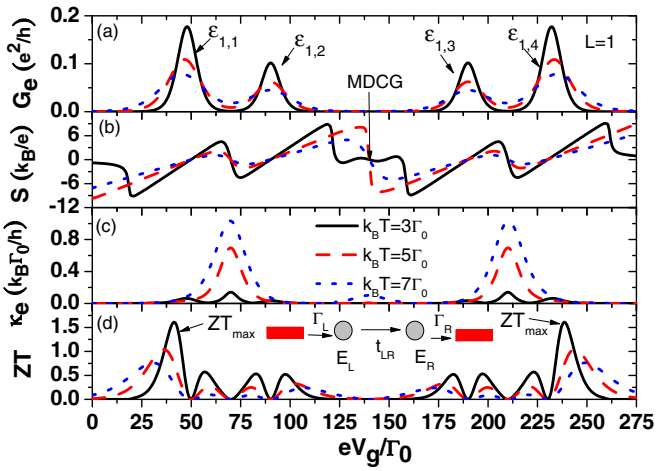

FIG. 5. (a) Electrical conductance (G_e), (b) Seebeck coefficient (S), (c) electron thermal conductance (κ_e), and (d) figure of merit (ZT) as a function of QD energy level tuned by gate voltage ($E_0 = E_F + 50\Gamma_0 - eV_g$) in a DQD junction with $L = 1$ for various temperatures. We have considered the electron hopping strength $t_{LR} = 1\Gamma_0$, interdot Coulomb interaction $U_{LR} = 40\Gamma_0$, intradot Coulomb interactions $U_L = U_R = 100\Gamma_0$, $\Gamma_L = \Gamma_R = 1\Gamma_0$, and $F_s = 0.1$.

Similar to the single QD $L = 1$ case in Fig. 1(d) the maximum ZT values occur at either the level-depletion regime or the full-charging regime as seen in Fig. 5(d). Here, the maximum ZT is close to 1.7 at $k_BT = 3\Gamma_0$ with $F_s = 0.1$.

To further understand the relationship between physical parameters and thermoelectric coefficients, we consider some approximations which include only the dominant correlation functions to derive $\mathcal{T}_{LR}(\epsilon)$ for DQD with $L = 1$. Simple analytic expressions of $G^{<}_{j,\sigma}(\epsilon), G^{r}_{j,\sigma}(\epsilon)$ and $G^{a}_{j,\sigma}(\epsilon)$ can be found in our previous work [42], when we only include intradot two-particle correlation functions in the probability weights. Here, we include all two-particle and three-particle correlation functions. Then, the following expression of $\mathcal{T}_{LR}(\epsilon)$ is obtained by solving the hierarchy of equations of motion (which terminates at the four-particle Green function) via a similar procedure as described in Ref. [42].

$$\begin{aligned}
&\mathcal{T}_{LR}(\epsilon)/\left(4t^2_{LR}\Gamma_L\Gamma_R\right) \\
&= \frac{P_{1,1}}{\left|\mu_L\mu_R - t^2_{LR}\right|^2} \\
&\quad + \frac{P_{1,2}}{\left|(\mu_L - U_{LR})(\mu_R - U_R) - t^2_{LR}\right|^2} \\
&\quad + \frac{P_{1,3}}{\left|(\mu_L - U_{LR})(\mu_R - U_{LR}) - t^2_{LR}\right|^2} \\
&\quad + \frac{P_{1,4}}{\left|(\mu_L - 2U_{LR})(\mu_R - U_{LR} - U_R) - t^2_{LR}\right|^2} \\
&\quad + \frac{P_{1,5}}{\left|(\mu_L - U_L)(\mu_R - U_{LR}) - t^2_{LR}\right|^2} \\
&\quad + \frac{P_{1,6}}{\left|(\mu_L - U_L - U_{LR})(\mu_R - U_R - U_{LR}) - t^2_{LR}\right|^2}
\end{aligned}$$

$$+\frac{P_{1,7}}{\left|(\mu_L-U_L-U_{LR})(\mu_R-2U_{LR})-t_{LR}^2\right|^2}+\frac{P_{1,8}}{\left|(\mu_L-U_L-2U_{LR})(\mu_R-U_R-2U_{LR})-t_{LR}^2\right|^2}, \quad (19)$$

where $\mu_L=\epsilon-E_L+i\Gamma_L$ and $\mu_R=\epsilon-E_R+i\Gamma_R$. The probability weights are given by $P_{1,1}=1-N_{L,\bar{\sigma}}-N_{R,\bar{\sigma}}-N_{R,\sigma}+\langle n_{L,\bar{\sigma}}n_{R,\bar{\sigma}}\rangle+\langle n_{L,\bar{\sigma}}n_{R,\sigma}\rangle+\langle n_{R,\bar{\sigma}}n_{R,\sigma}\rangle-\langle n_{L,\bar{\sigma}}n_{R,\bar{\sigma}}n_{R,\sigma}\rangle$, $P_{1,2}=N_{R,\bar{\sigma}}-\langle n_{L,\bar{\sigma}}n_{R,\bar{\sigma}}\rangle-\langle n_{R,\bar{\sigma}}n_{R,\sigma}\rangle+\langle n_{L,\bar{\sigma}}n_{R,\bar{\sigma}}n_{R,\sigma}\rangle$, $P_{1,3}=N_{R,\sigma}-\langle n_{L,\bar{\sigma}}n_{R,\sigma}\rangle-\langle n_{R,\bar{\sigma}}n_{R,\sigma}\rangle+\langle n_{L,\bar{\sigma}}n_{R,\bar{\sigma}}n_{R,\sigma}\rangle$, $P_{1,4}=\langle n_{R,\bar{\sigma}}n_{R,\sigma}\rangle-\langle n_{L,\bar{\sigma}}n_{R,\bar{\sigma}}n_{R,\sigma}\rangle$, $P_{1,5}=N_{L,\bar{\sigma}}-\langle n_{L,\bar{\sigma}}n_{R,\bar{\sigma}}\rangle-\langle n_{L,\bar{\sigma}}n_{R,\sigma}\rangle+\langle n_{L,\bar{\sigma}}n_{R,\bar{\sigma}}n_{R,\sigma}\rangle$, $P_{1,6}=\langle n_{L,\bar{\sigma}}n_{R,\bar{\sigma}}\rangle-\langle n_{L,\bar{\sigma}}n_{R,\bar{\sigma}}n_{R,\sigma}\rangle$, $P_{1,7}=\langle n_{L,\bar{\sigma}}n_{R,\sigma}\rangle-\langle n_{L,\bar{\sigma}}n_{R,\bar{\sigma}}n_{R,\sigma}\rangle$, and $p_{1,8}=\langle n_{L,\bar{\sigma}}n_{R,\bar{\sigma}}n_{R,\sigma}\rangle$, where $\langle n_{\ell,\bar{\sigma}}n_{j,\sigma}\rangle$ denote the two particle correlation functions and $\langle n_{\ell,\bar{\sigma}}n_{j,\sigma}n_{j,\bar{\sigma}}\rangle$ the three-particle correlation functions (including both intradot and interdot terms). Note that the probability weights satisfy the conservation law $\sum_m P_{1,m}=1$. $U_{L(R)}$ and $U_{L,R}$ denote the intradot and interdot Coulomb interactions. When all correlation functions of DQDs are included as in Refs. [21,40], it is difficult to find an analytical expression for $\mathcal{T}_{LR}(\epsilon)$. The thermoelectric coefficients, G_e, S, κ_e, and ZT obtained by using Eq. (19) are plotted in Fig. 6. The results are in very good agreement with those shown in Fig. 5, which are obtained by the full calculation, including all correlation functions. It should be noted that Eq. (19) works well only in the limit $t_{LR}/k_BT\ll 1$. If one would like to study the spin-dependent thermoelectric coefficients of DQD in the low temperature regime ($k_BT<t_{LR}$), all correlations functions should be included [40].

In Figs. 5 and 6, the peak positions $\epsilon_{1,n}$ ($n=1,2,3,4$) correspond to the channels with probability weights $P_{1,1}$, $P_{1,3}$, $P_{1,6}$, and $P_{1,8}$, respectively. There exists an interesting behavior for S at low temperature ($k_BT=3\Gamma_0$). We found that S is a linear function of eV_g near the maximum of G_e. From the κ_e behavior shown in Figs. 5(c) and 6(c), the electron heat flow is maximized near the midpoint between the first (or last) two resonant channels, and it increases with increasing temperature. Equation (19) allows us to obtain an analytic form of thermoelectric coefficients, which is very useful for clarifying how thermoelectric coefficients are influenced by tunneling rates, interdot hopping strength, and electron Coulomb interactions. Our analysis shows that S is independent of t_{LR} and it has a linear dependence of $\Delta=E_0-E_F$ [see Eqs. (21) and (22)] near maximum ZT. As a consequence, the trend of ZT with respect to t_{LR} is determined by that of G_e for $\kappa_{ph}/\kappa_e\gg 1$.

Next we consider the case with twofold degenerate levels ($L=2$) for each QD in the DQD junction. Such twofold degeneracy can be realized in QDs with suitable symmetry. For example, the x- and y-like states in a disk-shaped QD are degenerate. Due to symmetry, the intradot electron hopping process is prohibited, whereas the interdot electron hopping strength is nonzero. We assume $t_{LR}=1\Gamma_0$, the same as that of the $L=1$ case. The intradot Coulomb interactions are taken to be $U_{L,i,j}=U_{R,i,j}=U_I=50\Gamma_0$, where $i,j=1,2$ denote the two degenerate levels within the same QD. The interdot Coulomb interaction is taken as $U_{L,R}=40\Gamma_0$. The calculation of thermoelectric coefficients of DQD with $L=2$ involves solving one-, two-, $\cdots$, up to eight-particle Green functions. Due to the presence of the t_{LR} term, the numerical procedure is much more complicated than that of a single QD with $L=4$. Based on Eqs. (4)–(6), we calculate the thermoelectrical coefficients of DOD for the $L=2$ as functions of the QD energy level as shown in Fig. 7. The first four resonant channels of G_e (on the left hand side of MDCG) are approximately given by $\epsilon_{2,1}=E_0$, $\epsilon_{2,2}=E_0+U_{LR}$, $\epsilon_{2,3}=E_0+U_{LR}+U_I$, and $\epsilon_{2,4}=E_0+2U_{LR}+U_I$, in which the small t_{LR} is neglected since $t_{LR}\ll U_{L,R}$. The oscillatory behavior of G_e displayed in Fig. 7(a) is similar to the G_e spectra observed experimentally

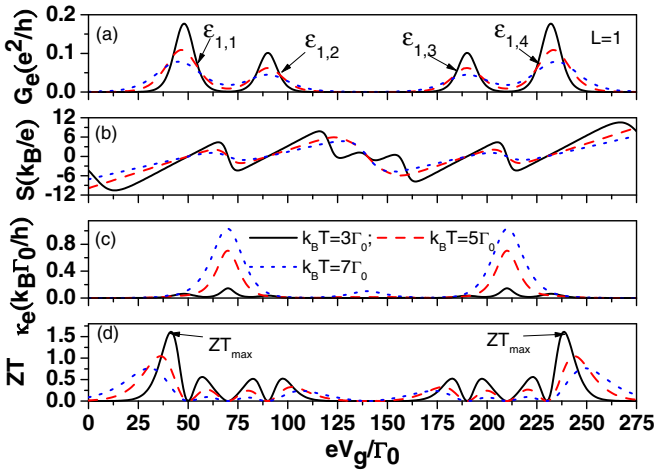

FIG. 6. (a) electrical conductance (G_e), (b) Seebeck coefficient (S), (c) electron thermal conductance (κ_e), and (d) figure of merit (ZT) as a function of QD energy level tuned by gate voltage ($E_0=E_F+50\Gamma_0-eV_g$) in a DQD junction with $L=1$ for various temperatures calculated by using Eq. (19). Other physical parameters are the same as those of Fig. 5.

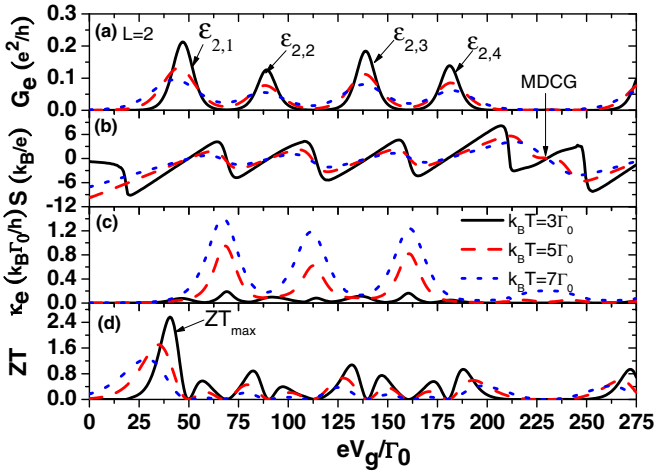

FIG. 7. (a) Electrical conductance (G_e), (b) Seebeck coefficient (S), (c) electron thermal conductance (κ_e), and (d) figure of merit (ZT) as a function of QD energy level tuned by gate voltage ($E_0=E_F+50\Gamma_0-eV_g$) in a DQD junction with $L=2$ for various temperatures. $U_{L,\ell,j}=U_{R,\ell,j}=50\Gamma_0$ and $U_{LR}=40\Gamma_0$. Other physical parameters are the same as those of Fig. 5.

in tunneling current measurements of PbSe QD (which has a sixfold degenerate excited state) and carbon nanotube QD (which has an eightfold state) [43,44]. Although the S spectrum exhibits more bipolar oscillatory structures, the maximum S value does not increase with increasing L. This feature is the same as that of a single QD case. Figure 7(d) shows a large enhancement of maximum ZT arising from the degeneracy effect. In the current case, $ZT_{\max}$ reaches around 2.7. Comparing Fig. 7(d) with Fig. 5(d), we see an enhancement of maximum ZT from around 1.7 to 2.7 when L increases from 1 to 2 for DQD junction when $F_s = 0.1$. We expect an even larger enhancement to occur for higher level degeneracy. Unfortunately, the computation effort for $L > 2$ for a DQD junction is prohibitively large if all Green functions and correlations functions are to be included.

To clarify the behavior of $ZT_{\max}$ in the level-depletion regime (with $N_t < 1$), we can approximately write (by keeping only the dominant channel)

$$\mathcal{T}_{LR}(\epsilon) \approx \frac{4\Gamma_L\Gamma_R t_{LR}^2 L P_{L,1}}{\left|(\epsilon - E_0 + i\Gamma_L)(\epsilon - E_0 + i\Gamma_R) - t_{LR}^2\right|^2}, \quad (20)$$

where $P_{L,1}$ is the probability weight for DQD in the level-depletion regime. Under the assumption of $\Gamma_L = \Gamma_R \to 0$ and $t_{LR}/k_BT \ll 1$, we have

$$\mathcal{L}_0 = \frac{2}{hk_BT}\frac{\pi\Gamma t_{LR}^2 L P_{L,1}}{\left(4t_{LR}^2 + \Gamma^2\right)}\frac{1}{\cosh^2\left(\frac{\Delta}{2k_BT}\right)} \quad (21)$$

and

$$\mathcal{L}_1 = \frac{2}{hk_BT}\frac{\pi\Gamma t_{LR}^2 L P_{L,1}}{\left(4t_{LR}^2 + \Gamma^2\right)}\frac{\Delta}{\cosh^2\left(\frac{\Delta}{2k_BT}\right)}. \quad (22)$$

From Eqs. (21) and (22), we have $G_e = e^2\mathcal{L}_0$ and $S = -\Delta/(eT)$. This reveals the behavior of S around the maximum of G_e at $k_BT = 3\Gamma_0$ in Fig. 6(b) and L-dependent $ZT_{\max}$ determined by G_e in Fig. 7(d). Note that if we artificially set $F_s = 0$ (i.e., neglecting κ_{ph}), one can prove that the enhancement of $ZT_{\max}$ arising from L will disappear due to the L independence of the ratio G_e/κ_e and L independence of S. If we choose a much higher value of F_s (e.g., $F_s = 1$) in Eq. (14), we will have the condition $\kappa_{ph}/\kappa_e \gg 1$. In this situation, L dependence of $ZT_{\max}$ is fully determined by G_e and we have ZT linearly proportional to L, since $P_{L,1}$ in Eq. (18) is close to 1 under the condition $(E_0 - E_F)/k_BT \gg 1$, and the ZT values will be approximately proportional to $1/F_s$. Finally, we would like to point out that QD junctions embedded in a silicon nanowire can be realized by the advanced technique reported in Refs. [45,46].

IV. CONCLUSION

We have theoretically investigated the effects of level degeneracy on thermoelectric properties of QDs embedded in a thin nanowire junction in the Coulomb blockade regime. All the correlation functions arising from electron Coulomb interactions for electrons in the degenerate levels are included in our calculation. We found that the maximum values of ZT can be highly enhanced with level degeneracy under the typical condition with κ_{ph} much larger than κ_e. When $(E_0 - E_F)/k_BT \gg 1$, S is independent of L. Therefore, the enhancement of $ZT_{\max}$ in the level-depletion regime is mainly attributed to the increase of G_e. Large enhancement of ZT due to the increase of level degeneracy is also found in the presence of finite electron hopping in coupled QD system. In our studies, we assumed a simple expression $\kappa_{ph} = F_s g_0(T)$ for the phonon thermal conductance. However, it is worth pointing out that our conclusion on the effect of level degeneracy on ZT is not limited to the linear T behavior of κ_{ph} (as illustrated in Fig. 4). The enhancement due to level degeneracy holds as long as $\kappa_{ph} > \kappa_e$, regardless of the temperature dependance of κ_{ph}. This implies that the design principle based increasing level degeneracy is applicable for composite materials involving arrays of coupled QDs [1,2] and molecular QDs [13].

ACKNOWLEDGMENTS

This work was supported by the Ministry of Science and Technology of Taiwan under Contracts No. MOST 103-2112-M-008-009-MY3 and No. MOST 104-2112-M-001-009-MY2.

[1] G. Chen, M. S. Dresselhaus, G. Dresselhaus, J. P. Fleurial and T. Caillat, Int. Mater. Rev. **48**, 45 (2003).
[2] A. J. Minnich, M. S. Dresselhaus, Z. F. Ren, and G. Chen, Energy Environ Sci. **2**, 466 (2009).
[3] R. Venkatasubramanian, E. Siivola, T. Colpitts, and B. O'Quinn, Nature (London) **413**, 597 (2001).
[4] A. I. Boukai, Y. Bunimovich, J. Tahir-Kheli, J. K. Yu, W. A. Goddard, III, and J. R. Heath, Nature (London) **451**, 168 (2008).
[5] T. C. Harman, P. J. Taylor, M. P. Walsh, and B. E. LaForge, Science **297**, 2229 (2002).
[6] Y. M. Lin and M. S. Dresselhaus, Phys. Rev. B **68**, 075304 (2003).
[7] K. F. Hsu, S. Loo, F. Guo, W. Chen, J. S. Dyck, C. Uher, T. Hogan, E. K. Polychroniadis, and M. G. Kanatzidis, Science **303**, 818 (2004).
[8] A. Majumdar, Science **303**, 777 (2004).
[9] C. R. Kagan and C. B. Murray, Nat. Nanotechnol. **10**, 1013 (2015).
[10] L. D. Hicks and M. S. Dresselhaus, Phys. Rev. B **47**, 12727 (1993).
[11] L. D. Hicks, and M. S. Dresselhaus, Phys. Rev. B **47**, 16631 (1993).
[12] D. L. Nika, E. P. Pokatilov, A. A. Balandin, V. M. Fomin, A. Rastelli, and O. G. Schmidt, Phys. Rev. B **84**, 165415 (2011).
[13] P. Murphy, S. Mukerjee, and J. Moore, Phys. Rev. B **78**, 161406(R) (2008).
[14] P. Trocha and J. Barnas, Phys. Rev. B **85**, 085408 (2012).
[15] R. Q. Wang, L. Sheng, R. Shen, B. G. Wang, and D. Y. Xing, Phys. Rev. Lett. **105**, 057202 (2010).
[16] G. Mahan, B. Sales and J. Sharp, Physics Today **50**(3), 42 (1997).
[17] H. Haug and A. P. Jauho, *Quantum Kinetics in Transport and Optics of Semiconductors* (Springer, Heidelberg, 1996).

[18] S. Datta, *Electronic Transport in Mesoscopic Systems* (Cambridge University Press, Cambridge, 1995).
[19] Y. Meir and N. S. Wingreen, Phys. Rev. Lett. **68**, 2512 (1992).
[20] C. C. Chen, Y. C. Chang, and D. M.-T. Kuo, Phys. Chem. Chem. Phys. **17**, 6606 (2015); C. C. Chen, Ph.D. thesis, University of Illinois at Urbana-Champaign, 2015, available at https://www.ideals.illinois.edu/handle/2142/88937.
[21] C. C. Chen, D. M.-T. Kuo, and Y. C. Chang, Phys. Chem. Chem. Phys. **17**, 19386 (2015).
[22] D. Li, Y. Y. Wu, P. Kim, L. Shi, P. D. Yang, and A. Majumdar, Appl. Phys. Lett. **83**, 2934 (2003).
[23] D. Li, Y. Y. Wu, R. Fan, P. D. Yang, and A. Majumdar, Appl. Phys. Lett. **83**, 3186 (2003).
[24] R. K. Chen, A. I. Hochbaum, P. Murphy, J. Moore, P. D. Yang, and A. Majumdar, Phys. Rev. Lett. **101**, 105501 (2008).
[25] M. C. Wingert, Z. C.-Y. Chen, E. Dechaumphai, J. Moon, J.-H. Kim, J. Xiang, and R. K. Chen, Nano Lett. **11**, 5507 (2011).
[26] A. I. Hochbaum, R. K. Chen, R. D. Delgado, W. Liang, E. C. Garnett, M. Najarian, A. Majumdar, and P. D. Yang, Nature (London). **451**, 163 (2008)
[27] N. Mingo and L. Yang, Phys. Rev. B **68**, 245406 (2003).
[28] P. G. Murphy and J. E. Moore, Phys. Rev. B **76**, 155313 (2007).
[29] D. Donadio and G. Galli, Phys. Rev. Lett. **102**, 195901 (2009).
[30] G. B. Akguc and J. Gong, Phys. Rev. B **80**, 195408 (2009).
[31] T. M. Gibbons, B. Kang, S. K. Estreicher and C. Carbogno, Phys. Rev. B **84**, 035317 (2011).
[32] E. B. Ramayya, L. N. Maurer, A. H. Davoody, and I. Knezevic, Phys. Rev. B **86**, 115328 (2012).
[33] T. Zhu and E. Ertekin, Phys. Rev. B **93**, 155414 (2016).
[34] K. Schwab, E. A. Henriksen, J. M. Worlock, and M. L. Roukes, Nature (London) **404**, 974 (2000).
[35] Y. Zhang, M. S. Dresselhaus, Y. Shi, Z. Ren, and G. Chen, Nano. Lett. **11**, 1166 (2011).
[36] T. Zhu and E. Ertekin, Phys. Rev. B **90**, 195209 (2014).
[37] T. Zhu and E. Ertekin, Nano Lett. **16**, 4763 (2016).
[38] D. M.-T. Kuo and Y. C. Chang, Phys. Rev. B **81**, 205321 (2010).
[39] B. Sothmann, R. Sanchez and A. N. Jordan, Nanotechnol. **26**, 032001 (2015).
[40] B. R. Bulka and T. Kostyrko, Phys. Rev. B **70**, 205333 (2004).
[41] B. Muralidharan and S. Datta, Phys. Rev. B **76**, 035432 (2007).
[42] D. M.-T. Kuo, S.-Y. Shiau, and Y.-C. Chang, Phys. Rev. B **84**, 245303 (2011).
[43] P. Liljeroth, L. Jdira, K. Overgaag, B. Grandidier, S. Speller, and D. Vanmaekelbergh, Phys. Chem. Chem. Phys. **8**, 3845 (2006).
[44] S. Moon, W. Song, J. S. Lee, N. Kim, J. Kim, S. G. Lee, and M. S. Choi, Phys. Rev. Lett. **99**, 176804 (2007).
[45] G. L. Chen, D. M. Kuo, W. T. Lai and P. W. Li, Nanotechnology **18**, 475402 (2007).
[46] J. W. Lee, J. Lee, S. H. Jung, Y. Jang, B. L. Choi, C. W. Yang, D. Whang, and E. K. Lee, Nanotechnology **27**, 305703 (2016).